Phases and Transitions in the Spin-1 Bose-Hubbard Model: Systematics of a Mean-field Theory

Ramesh V. Pai[*]

Department of Physics, Goa University, Taleigao Plateau, Goa 403 206, India.

K. Sheshadri[†]

686, BEL Layout, 3rd Block, Vidyaranyapura, Bangalore 560 097, India.

Rahul Pandit[‡]

*Centre for Condensed Matter Theory, Department of Physics,
Indian Institute of Sciences, Bangalore 560 012, India.*

(Dated: February 1, 2008)

We generalize the mean-field theory for the spinless Bose-Hubbard model to account for the different types of superfluid phases that can arise in the spin-1 case. In particular, our mean-field theory can distinguish polar and ferromagnetic superfluids, Mott insulators which arise at integer fillings at zero temperature, and normal Bose liquids into which the Mott insulators evolve at finite temperatures. We find, in contrast to the spinless case, that several of the superfluid-Mott insulator transitions are first-order at finite temperatures. Our systematic study yields rich phase diagrams that include, first-order and second-order transitions, and a variety of tricritical points. We discuss the possibility of realizing such phase diagrams in experimental systems.

I. INTRODUCTION

Experimental investigations of ultracold atoms in optical lattices have opened up a new realm in the study of quantum phase transitions (QPT)[1,2]. The superfluid (SF) to Mott-insulator (MI) transition has been observed in spin-polarized ^{87}Rb atoms trapped in a three-dimensional, optical-lattice potential[3], by changing the strength of the onsite potential, as predicted theoretically by studies of the spinless Bose-Hubbard model[4,5]. Furthermore, technical advances in the trapping of atoms by purely optical means[6] have enhanced the interest in the study of quantum magnetism in confined dilute atomic gases. Alkali atoms with nuclear spin $I = 3/2$, such as ^{23}Na, ^{39}K, and ^{87}Rb, have hyperfine spin $F = 1$. In conventional *magnetic traps*, these spins are frozen, so the atoms can be treated as spinless bosons; by contrast, in *purely optical traps*, these spins are free, so the Bose condensates, which form at low temperatures, can have a spinor nature[7,8] and the SF-MI transition can be modified[9,10,11]. In the spinless case, the SF-MI transitions are controlled by the interaction U_0 between bosons at the same site. As U_0 increases beyond a critical value, the SF phase undergoes a continuous transition to an MI phase in which the number of bosons at every site is an integer. This transition is reflected in the development of a gap at the transition. When the spin is nonzero such a gap also develops at SF-MI transitions, but the properties of the phases and the natures of these transitions are modified by the spin degrees of freedom.

Theoretical work on this problem has dealt primarily with the properties of spinor condensates by using a continuum, effective, low-energy Hamiltonian. Such a Hamiltonian suffices if one is interested in the natures of the superfluid phases, which can be polar or ferromagnetic, and in their excitations, which include vector or quadrupolar spin waves and topological defects[7,8]. However, if we want to study the SF-MI transitions we must use a lattice model such as the spin-one Bose-Hubbard model. Some groups[9,10,11] have initiated such an investigation by obtaining the zero-temperature phase diagram of this model in a mean-field approximation. The topology of this phase diagram for the spin-1 Bose-Hubbard model is similar to that of its spinless counterpart; but, in the spin-1 model, the superfluid phases can be either polar or ferromagnetic depending on whether the spin-dependent interaction favors or disfavors the formation of singlets. In the former case the SF-MI phase transition is *continuous*, if the density of bosons per site ρ is an odd number, but *first-order*, if ρ is an even number.

We have two main goals in this paper: The first is to give a global view of the zero-temperature, mean-field-theory phase diagram of the spin-1 Bose Hubbard model emphasizing issues of first-order coexistence that have not been highlighted so far. The second is to generalize this mean-field theory to finite temperatures $T > 0$ and thus obtain the finite-temperature, mean-field-theory phase diagram for this model.

The spin-1 Bose-Hubbard model is defined by the Hamiltonian

$$\mathcal{H} = -t \sum_{<i,j>,\sigma} (a_{i,\sigma}^{\dagger} a_{j,\sigma} + h.c) + \frac{U_0}{2} \sum_i \hat{n}_i (\hat{n}_i - 1)$$
$$+ \frac{U_2}{2} \sum_i (\vec{F}_i^2 - 2\hat{n}_i) - \sum_i \mu_i \hat{n}_i, \tag{1}$$

where the first is the kinetic energy associated with the hopping of bosons between nearest-neighbor pairs of sites

$< i, j >$ with amplitude t, $a_{i,\sigma}^{\dagger}$ $(a_{i,\sigma})$ is the boson creation (annihilation) operator at site i with spin component σ (which can assume the values $1, 0, -1$), $\hat{n}_{i\sigma} \equiv a_{i,\sigma}^{\dagger} a_{i,\sigma}$; $\hat{n}_i \equiv \sum_{\sigma} \hat{n}_{i,\sigma}$ and $\vec{F}_i = \sum_{\sigma,\sigma'} a_{i,\sigma}^{\dagger} \vec{F}_{\sigma,\sigma'} a_{i,\sigma'}$ are, respectively, the total boson number and spin on site i, and $\vec{F}_{\sigma,\sigma'}$ are the standard spin-one matrices; U_0 is the on-site Hubbard repulsion and U_2 the energy for nonzero spin configurations on a site. The origin of such a spin-dependent term lies in the difference between the scattering lengths a_0 and a_2, for $S = 0$ and $S = 2$ channels[12], respectively; in terms of these lengths $U_0 = 4\pi\hbar^2(a_0 + 2a_2)/3M$ and $U_2 = 4\pi\hbar^2(a_2 - a_0)/3M$, where M is the mass of the atom[7]. For ^{23}Na, $a_2 = 54.7a_B$ and $a_0 = 49.4a_B$, where a_B is the Bohr radius, so $U_2 > 0$, whereas for ^{87}Rb, $a_2 = (107\pm4)a_B$ and $a_0 = (110\pm4)a_B$, so U_2 can be negative. The parabolic trapping potential with strength V_T is represented by the site-dependent chemical potential $\mu_i = \mu - V_T|R_i|^2$, where R_i is the distance of site i from the center of the trap and μ is a uniform chemical potential that controls the mean density of the bosons. In this study we neglect the trap potential (i.e., we set $V_T = 0$) and focus on the effects of the spin degrees of freedom.

The zero-temperature phase diagram of model (1) has been obtained in the mean-field approximation by some groups[9,10,11]. We have extended these studies significantly. Before presenting the details of our work, we give a qualitative overview of our new results.

Consider first the case $U_2 = 0$: We might expect the spin-1 and spinless Bose-Hubbard models to have same phase diagram in this case since the ground-state energy does not depend on the spin. This is superficially true at $T = 0$ in so far as the SF-MI phase boundaries for both these models overlap. However, as we will show, the SF phase is highly degenerate in the spin-1 case; and for $T > 0$ the SF-MI transition becomes first-order and, eventually, continuous again. Thus the finite-temperature phase diagram has a rich topology with first-order boundaries evolving into continuous ones at tricritical points.

If $U_2 \neq 0$ the onsite interaction between the bosons becomes spin dependent. It turns out that we must distinguish between the cases $U_2 < 0$ and $U_2 > 0$. The former yield a phase diagram that is very similar to the one for $U_2 = 0$; the major qualitative difference arises in the nature of the SF phase that is now a ferromagnetic superfluid.

There are many differences between the phase diagrams of the spin-1 model with $U_2 = 0$ and $U_2 > 0$. If $U_2 > 0$ the SF phase is a polar superfluid. Furthermore, even at $T = 0$, the SF-MI transitions are different for odd and even densities. For odd densities, the $T = 0$ SF-MI transition is continuous as for $U_2 = 0$; however, for even densities, this SF-MI transition turns out to be first-order because of the formation of singlets that also stabilize the MI phase considerably.

At finite temperatures the MI phases evolve without

a singularity into a normal Bose liquid (NBL). These are really not distinct phases but, as we will show, the compressibility κ can be used effectively to delineate the crossover between MI and NBL regions.

To present our results in detail we must introduce our mean-field theory. We do this in Sec. II. Our results are given in Sec. III. We end with a discussion in Sec. IV.

II. MEAN-FIELD THEORY

Mean-field theory has been very successful in obtaining the phase diagram for the spinless Bose-Hubbard model. There are three formulations of this mean-field theory: one uses a model with infinite-range interactions, another a Gutzwiller-type wave function, and a third[5], which we follow, a decoupling approximation. The unique feature of this decoupling scheme is that, unlike conventional mean-field theories, it does not decouple the interaction term to obtain an effective, *one-particle* problem but, instead, decouples the hopping term to obtain an effective, *one-site* problem. This one-site problem is then solved self-consistently. We generalize this decoupling procedure to the spin-1 case as follows[5]: In the identity $a_{i,\sigma}^{\dagger} a_{j,\sigma} = (a_{i,\sigma}^{\dagger} - \langle a_{i,\sigma}^{\dagger} \rangle)(a_{j,\sigma} - \langle a_{j,\sigma} \rangle) + \langle a_{i,\sigma}^{\dagger} \rangle a_{j,\sigma} + a_{i,\sigma}^{\dagger} \langle a_{j,\sigma} \rangle - \langle a_{i,\sigma}^{\dagger} \rangle \langle a_{j,\sigma} \rangle$, where $\langle \mathcal{O} \rangle$ denotes the equilibrium value of an operator $\mathcal{O}$, we neglect the first term that is quadratic in deviations from the equilibrium value. Thus

$$a_{i,\sigma}^{\dagger} a_{j,\sigma} \simeq \langle a_{i,\sigma}^{\dagger} \rangle a_{j,\sigma} + a_{i,\sigma}^{\dagger} \langle a_{j,\sigma} \rangle - \langle a_{i,\sigma}^{\dagger} \rangle \langle a_{j,\sigma} \rangle; \qquad (2)$$

since we expect superfluid phases, it is natural to introduce the superfluid order parameters

$$\psi_{\sigma} \equiv \langle a_{i,\sigma}^{\dagger} \rangle \equiv \langle a_{i,\sigma} \rangle, \qquad (3)$$

for $\sigma = 1, 0, -1$. We consider equilibrium states with uniform phases, so we choose these order parameters to be real. Given the decoupling approximation (2) the Hamiltonian (1) can be written as a sum over single-site, mean-field Hamiltonians:

$$\mathcal{H} = \sum_i \mathcal{H}_i^{MF}, \qquad (4)$$

where

$$\mathcal{H}_i^{MF} = \frac{U_0}{2}\hat{n}_i(\hat{n}_i - 1) + \frac{U_2}{2}(\vec{F}_i^2 - 2\hat{n}_i) - \mu\hat{n}_i$$
$$- \psi_{\sigma}(a_{i,\sigma}^{\dagger} + a_{i,\sigma}) + \sum_{\sigma} |\psi_{\sigma}|^2. \qquad (5)$$

We set the energy scale by choosing $zt = 1$, where z is the number of nearest neighbors. At least one of the order parameters ψ_{σ} is nonzero in a superfluid phase. In order to calculate ψ_{σ} in our mean-field theory, we first obtain the matrix elements of the mean-field Hamiltonian $\mathcal{H}_i^{MF}$

in the onsite, occupation-number basis $\{|n_{-1}, n_0, n_1 >\}$ truncated at a finite value $n_{\max}$ of the total number of bosons per site $n = \sum_\sigma n_\sigma$. In most of our studies we use $n_{max} = 4$ for which the mean-field Hamiltonian is a 36×36 matrix[13]. We diagonalize this matrix to obtain its eigenvalues $\mathcal{E}_\alpha$ and eigenvectors $|\varphi_\alpha\rangle$:

$$\mathcal{H}_i^{MF}|\varphi_\alpha\rangle = \mathcal{E}_\alpha|\varphi_\alpha\rangle; \qquad (6)$$

we suppress the site index i on these eigenvalues and eigenvectors since all the phases we consider are spatially uniform.

We now obtain the variational the free energy

$$\mathcal{F}(\mu, U_0, U_2, T; \psi_\sigma) = -T \ln Z(\mu, U_0, U_2, T; \psi_\sigma), \quad (7)$$

where $Z(\mu, U_0, U_2, T; \psi_\sigma)$ is the partition function

$$Z(\mu, U_0, U_2, T; \psi_\sigma) = \sum_\alpha e^{-\mathcal{E}_\alpha/T}, \qquad (8)$$

with the Boltzmann constant k_B chosen to be 1. The variational free energy $\mathcal{F}$ must be minimized with respect to the order parameters ψ_σ, i.e., we must solve the equations $\partial\mathcal{F}/\partial\psi_\sigma = 0$ for $\sigma = 1, 0, -1$. These equations can be recast as self-consistency conditions for ψ_σ; solutions of these self-consistency conditions correspond to extrema of $\mathcal{F}$. In case there is more than one solution, we must pick the one that yields the global minimum of $\mathcal{F}$. [At a first-order phase boundary $\mathcal{F}$ has two, equally deep, global minima.] The values of ψ_σ and $\mathcal{F}$ at the global minimum yield the equilibrium order parameters ψ_σ^{eq} and free energy $\mathcal{F}^{eq}$. In our mean-field theory, the superfluid density is

$$\rho_s = \sum_\sigma |\psi_\sigma^{eq}|^2 . \qquad (9)$$

The magnetic properties of the superfluid phases of this model are obtained from [7]

$$\langle\vec{F}\rangle = \frac{\sum_{\sigma,\sigma'} \psi_\sigma^{eq} \vec{F}_{\sigma,\sigma'} \psi_{\sigma'}^{eq}}{\sum_\sigma |\psi_\sigma^{eq}|^2}; \qquad (10)$$

the explicit forms of the spin-1 matrices now yield

$$\langle\vec{F}\rangle = \sqrt{2}\frac{(\psi_1\psi_0 + \psi_{-1}\psi_0)}{\sum_\sigma |\psi_\sigma|^2}\hat{x} + \frac{(\psi_1^2 - \psi_{-1}^2)}{\sum_\sigma |\psi_\sigma|^2}\hat{z},$$

$$\langle\vec{F}\rangle^2 = 2\frac{(\psi_1\psi_0 + \psi_{-1}\psi_0)^2}{(\sum_\sigma |\psi_\sigma|^2)^2} + \frac{(\psi_1^2 - \psi_{-1}^2)^2}{(\sum_\sigma |\psi_\sigma|^2)^2}, \quad (11)$$

where $\hat{x}$ and $\hat{z}$ are unit vectors in spin space and we suppress the superscript eq for notational convenience; all ψ_σ used here and henceforth are actually ψ_σ^{eq}. Superfluid states with $\langle\vec{F}\rangle = 0$ and $\langle\vec{F}\rangle^2 = 1$ are referred to as polar and ferromagnetic, respectively. The polar state[8] has an order-parameter manifold $(U(1) \times S^2)/\mathbb{Z}_2$, where $U(1)$ denotes the phase angle θ, S^2 refers to the directions $\hat{\mathbf{n}}$ on the surface of a unit sphere (on which orientations are specified by the angles (α, β) of the spin quantization

axis), and $\mathbb{Z}_2$ arises because of the symmetry of this state under the simultaneous transformations $\theta \to \theta + \pi$ and $\hat{\mathbf{n}} \to -\hat{\mathbf{n}}$. Thus the superfluid order parameters can be written as

$$\begin{pmatrix} \psi_1 \\ \psi_0 \\ \psi_{-1} \end{pmatrix} = \sqrt{\rho_s}e^{\imath\theta} \begin{pmatrix} -\frac{1}{\sqrt{2}}e^{-\imath\alpha}\sin\beta \\ \cos\beta \\ \frac{1}{\sqrt{2}}e^{\imath\alpha}\sin\beta. \end{pmatrix}. \qquad (12)$$

Similarly, since the ferromagnetic superfluid state has an order-parameter manifold[8] with the symmetry group $SO(3)$,

$$\begin{pmatrix} \psi_1 \\ \psi_0 \\ \psi_{-1} \end{pmatrix} = \sqrt{\rho_s}e^{\imath(\theta-\tau)} \begin{pmatrix} e^{-\imath\alpha}\cos^2\frac{\beta}{2} \\ \sqrt{2}\cos\frac{\beta}{2}\sin\frac{\beta}{2} \\ e^{\imath\alpha}\sin^2\frac{\beta}{2} \end{pmatrix}, \qquad (13)$$

where α, β, and τ are Euler angles.

We consider only spatially uniform superfluids in equilibrium, so it suffices to use real order parameters. Thus, for the polar superfluid we have the following possibilities: (i) $\psi_1 = \psi_{-1} > 0$ and $\psi_0 = 0$ with $\theta = \alpha = \beta = \pi/2$ or $\theta = -\alpha = \beta = \pi/2$; and (ii) $\psi_1 = \psi_{-1} = 0$ and $\psi_0 > 0$ with $\beta = 0$ or π, $\theta = 0$ or π, and $0 \leq \alpha \leq 2\pi$. Similarly for the ferromagnetic superfluid $\psi_1 = \psi_{-1}$, $\beta = \pi/2$, $\alpha = 0$, $0 \leq \theta = \tau \leq 2\pi$, and $\psi_0 = \sqrt{2}\psi_1$.

The equilibrium density ρ and compressibility κ can be obtained from

$$\rho = -\frac{\partial\mathcal{F}^{eq}}{\partial\mu} = \frac{1}{Z}\sum_\alpha e^{-E_\alpha/T}\langle\phi_\alpha | \hat{n} | \phi_\alpha\rangle, \qquad (14)$$

where E_α and $|\phi_\alpha\rangle$ are $\mathcal{E}_\alpha$ and $|\varphi_\alpha\rangle$ at the global minimum of $\mathcal{F}$ and

$$\kappa = \frac{\partial\rho}{\partial\mu}. \qquad (15)$$

The three quantities ρ_s, $\langle\vec{F}\rangle^2$, and κ together determine the thermodynamic phase of model (1) for any point in the parameter space $\{\mu, U_0, U_2, T\}$ as given in the Table I. Strictly speaking there is no distinction between the Mott insulator (MI) and the normal Bose liquid (NBL); the former exists at $T = 0$ and has $\kappa = 0$; it evolves without any singularity into the NBL at $T > 0$; at low T, the compressibility κ is exponentially small in the NBL so one can think of it as an MI phase; at high T, where κ is substantially different from 0, it is best to think of this phase as a normal Bose liquid. It is convenient, therefore, to define a crossover boundary above which κ is substantial; we use the criterion $\kappa = \kappa_X = 0.02$ to obtain the MI-NBL crossover boundary shown in some of our phase diagrams. We must remember of course that this is not a strict phase boundary and it depends on the value we choose for the crossover compressibility κ_X.

III. RESULTS

We are now in a position to present the results of our mean-field theory. It is necessary to distinguish between

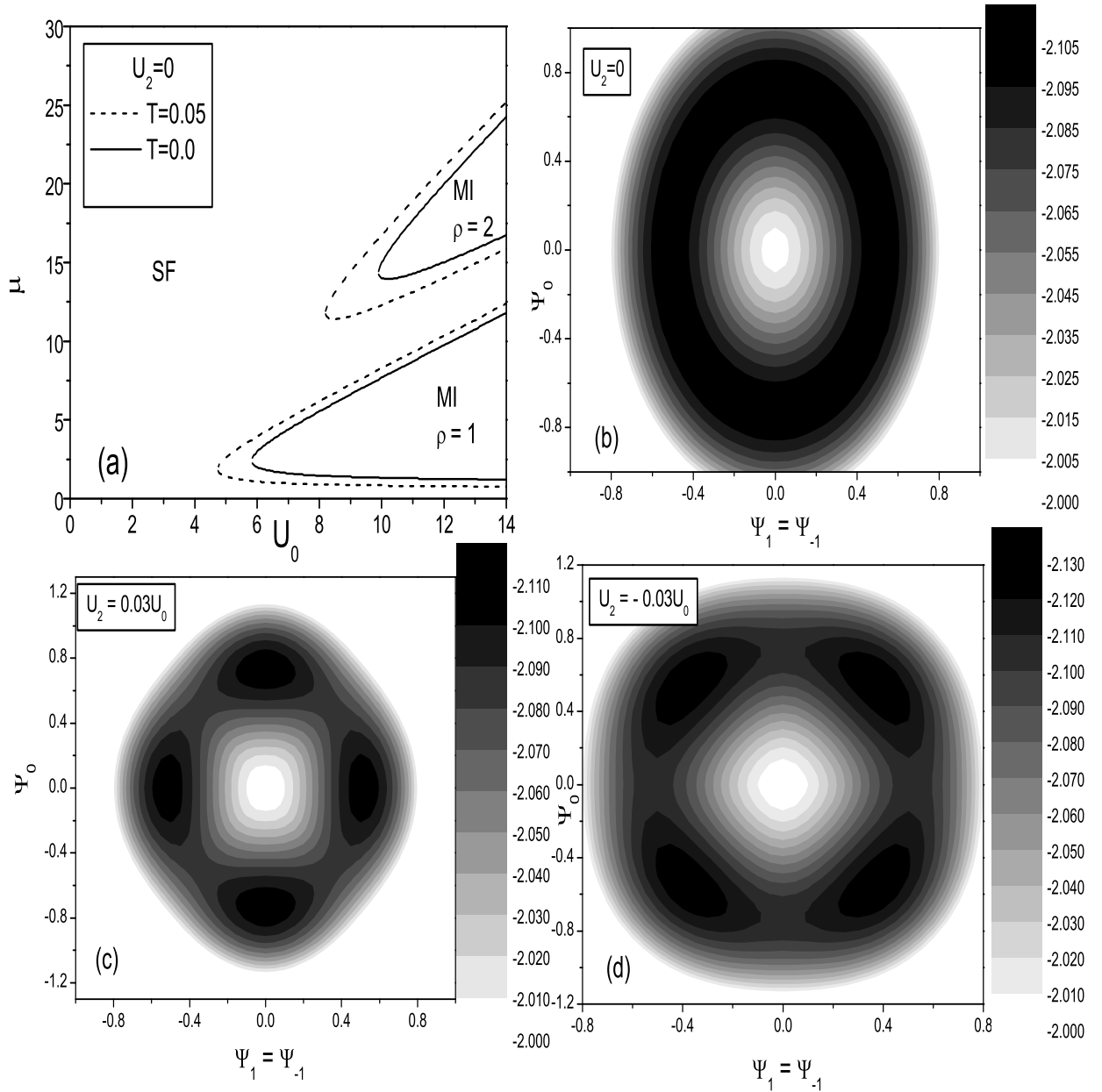FIG. 1: (a) Phase diagrams in the $(\mu - U_0)$ plane for $U_2 = 0$: Solid lines indicate the $T = 0$ continuous phase boundaries between SF and MI phases; these phase boundaries evolve into first-order boundaries at finite (but low) temperatures as shown by the representative dashed lines for $T = 0.05$; at higher temperatures these first-order boundaries become continuous again at lines of tricritical points. Pseudo-grayscale plots at $T = 0$ of the variational ground-state energy $\mathcal{E}_0$ for (b) $U_2 = 0$, (c) $U_2/U_0 = 0.03$, and (d) $U_2/U_0 = -0.03$, respectively; the four degenerate minima in (c) and (d) show that the SF phase is polar in the former and ferromagnetic in the latter; in case (b), i.e., $U_2 = 0$, the SF phase is infinitely degenerate (see text).
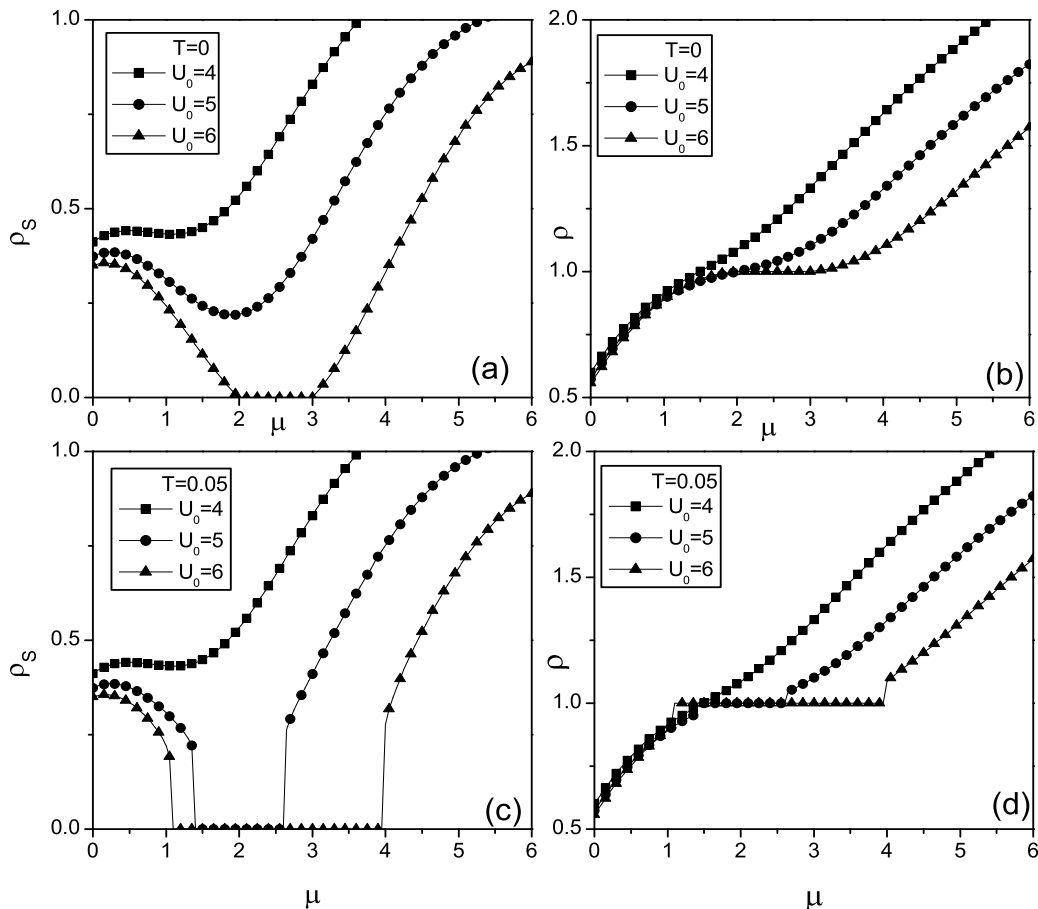
FIG. 2: Representative plots of (a) ρ_s and (b) ρ versus μ for $U_0 = 4, 5, 6$, $U_2 = 0$ at $T = 0$. Similar plots at $T = 0.05$ are given in (c) and (d). In the MI phases $\rho_s = 0$ and ρ is an integer [$= 1$ in (b) for $U_0 = 6$] for $T = 0$; for $0 \lesssim T$ the MI phase evolves without a singularity (see text) into the normal Bose liquid (NBL) in which ρ is exponentially close to an integer [$= 1$ in (d) for $U_0 = 5, 6$]. As the temperature increases from zero, the MI phases grow at the expense of SF phase and the SF-MI transition becomes first order [see Fig.(1].

three qualitatively different regimes: (1) $U_2/U_0 = 0$; (2) $U_2/U_0 > 0$ (we use $U_2/U_0 = 0.03$ since this is appropriate for ^{23}Na); and (3) $U_2/U_0 < 0$, as in ^{87}Rb (for specificity we use $U_2/U_0 = -0.03$).

We first consider $U_2/U_0 = 0$, which can be achieved when the scattering lengths are equal, i.e., $a_0 = a_2$. In this case the onsite interaction between bosons is spin independent. This leads to an infinitely degenerate superfluid state: Specifically, for a given value of the superfluid density ρ_s, the three order parameters $\psi_\sigma, \sigma = -1, 0, 1$, can have any magnitudes that satisfy Eq. (9); e.g., if we make the specific choice $\psi_{-1} = \psi_1$, then the pseudo-grayscale plot of Fig. 1 (b) shows that the minima of the variational mean-field energy at $T = 0$ lie on the ellipse $2\psi_1^2 + \psi_0^2 = \rho_s$. This degeneracy makes the superfluid phase of the spin-1 Bose-Hubbard model different from

its spin-0 counterpart *even if* $U_2 = 0$; and it implies that an infinite number of SF phases *coexist* at $U_2 = 0$. However, the zero-temperature phase diagram of Fig. 1 (a) is the same as that of the spinless Bose-Hubbard model[5]; and, in particular, lobes of the MI phase are separated from the SF phase by the SF-MI boundaries that are all continuous at $T = 0$; the density ρ is fixed at integral values in each MI lobe.

Striking differences between the spin-1 and spinless cases appear at finite temperatures. We demonstrate this in Figs. 1(a) and 2; the former compares phase diagrams at $T = 0$ and $T = 0.05$ and the latter presents plots, both at $T = 0$ and $T = 0.05$, of the superfluid density ρ_s and the density ρ as functions of the chemical potential μ for three different values of the onsite interaction U_0 ($= 4, 5, 6$). [In both spinless and spin-1 cases, if $U_2 = 0$,

Phases	ρ_s	$\langle \vec{F} \rangle^2$	κ
Polar Superfluid (PSF)	> 0	0	> 0
Ferro Sperfluid (FSF)	> 0	1	> 0
Mott Insulator (MI)	0	—	0
Normal Bose Liquid (NBL)	0	—	> 0

TABLE I: The superfluid density ρ_s, $\langle \vec{F} \rangle^2$, and the compressibility κ in the different phases of the spin-1 Bose-Hubbard model. The MI and NBL are really the same phase (see text).
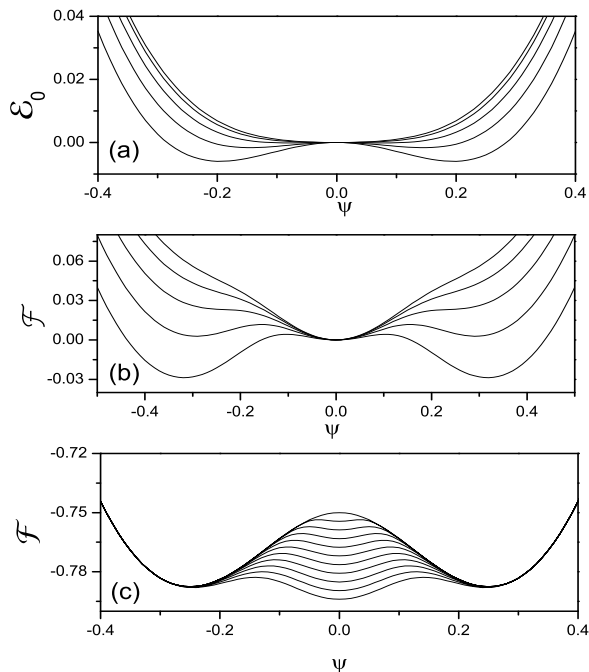

FIG. 3: Plots of the variational free energy $\mathcal{F}$ (ground-state energy $\mathcal{E}_0$ for $T = 0$) as a function of ψ for different values of μ in the vicinity of the SF-MI transition for $U_2 = 0$ and with $\psi_{-1} = \psi_0 = \psi_1 \equiv \psi$ (see text). The minima at $\psi = 0$ and $\psi \neq 0$ correspond, respectively, to MI and SF phases. (a) The two minima at $\psi \neq 0$ merge into one minimum at $\psi = 0$ to yield the mean-field continuous SF-MI transition at $T = 0$ as we increase μ from 1.5 (bottom curve) to 2.3 (top curve) in steps of 0.2. Similar plots of $\mathcal{F}$ are given in (b) and (c). For $0 \lesssim T$, $\mathcal{F}$ develops three degenerate minima at the SF-MI boundary, indicating clearly the coexistence of SF and MI phases at a first-order boundary. This boundary can be crossed either (b) by changing μ (from 0.7 to 1.5 in steps of 0.2) at fixed $T = 0.05$ or (c) by changing T (0 to 0.1 in steps of 0.01) at fixed $\mu = 2$.

the tip of the first lobe[5,11] lies at $U_{0c}(\rho = 1) \simeq 5.8$ for $T = 0$.] Figure 1 (a) shows that $U_{0c}(\rho)$ decreases as the T increases, i.e., the MI lobes grow at the expense of the SF phase. Figure 2 shows that ρ_s goes to zero continuously at the SF-MI transition, if $T = 0$, but with a jump if $T = 0.05$. Thus the SF-MI transition becomes a first-order transition at finite T and the zero-temperature SF-MI boundaries [Fig. 1 (a)]are really lines of tricritical points; as the temperature is increased further, the first-order transition again becomes continuous at another tricritical point.

The first-order, SF-MI coexistence boundary is associated with the three-degenerate-minima structure in the variational-free-energy plots shown in Fig. 3. To obtain these plots we use $\psi_{-1} = \psi_0 = \psi_1 \equiv \psi$ that is one of the admissible solutions in the infinitely degenerate SF phase for the case $U_2 = 0$; the infinite degeneracy of this phase, illustrated for $T = 0$ in Fig. 1 (b), persists in our mean-field theory even if $T > 0$. Figure 3 shows plots of the variational free energy $\mathcal{F}$ (ground-state energy $\mathcal{E}_0$ for $T = 0$) as a function of ψ for different values of μ in the vicinity of the SF-MI transition; the minima at $\psi = 0$ and $\psi \neq 0$ correspond, respectively, to MI and SF phases. At $T = 0$ the SF-MI transition is continuous: this is reflected in the plots of $\mathcal{E}_0$ in Fig. 3 (a), where, as we go from the SF to the MI phase by changing μ, two global minima with $\psi \neq 0$ merge to yield one minimum at $\psi = 0$; precisely at the mean-field critical point we have a *quartic* minimum. For $0 \lesssim T$, $\mathcal{F}$ develops three degenerate minima at the SF-MI boundary, indicating clearly the coexistence of SF and MI phases at a first-order boundary. This boundary can be crossed either by changing μ at fixed T [Fig. 3 (b)] or by changing T at fixed μ [Fig. 3 (c)]. At sufficiently high temperatures this three-minima structure of $\mathcal{F}$ goes away at a tricritical point at which the three minima coalesce to yield a *sixth-order* minimum. Beyond this tricritical point the SF-MI transition is continuous (second-order).

Calculations such as those summarized in the plots of Fig. 3 help us to obtain the phase diagrams shown in Figs. 4 (a) - (d) for $U_0 = 12$ and $U_2 = 0$. Let us begin with the $\mu - T$ phase diagram shown in Fig. 4 (a). The MI phases [lobes in Fig. 1 (a)] at $T = 0$ evolve without any singularity into the normal Bose liquid (NBL) for $T > 0$. As we have emphasized earlier, MI and NBL phases are not distinct, but it is useful to think of a smooth crossover from one to the other; we define these crossover boundaries as the loci of points at which the compressibility $\kappa = \kappa_x = 0.02$. The MI-NBL crossover boundaries (lines with filled triangles) are also shown in Figs. 4 (a) and (c). Islands of the SF phase appear in the $\mu - T$ phase diagram; the first two of these are shown in Fig. 4 (a), where one is marked SF and the other, near the origin, is shown magnified in Figs. 4 (b) and (c). The only difference between Figs. 4 (b) and (c) is that the latter shows the MI-NBL crossover boundary (line with triangles) and a line with stars, the locus of points in the SF phase at which the variational free energy $\mathcal{F}$ goes
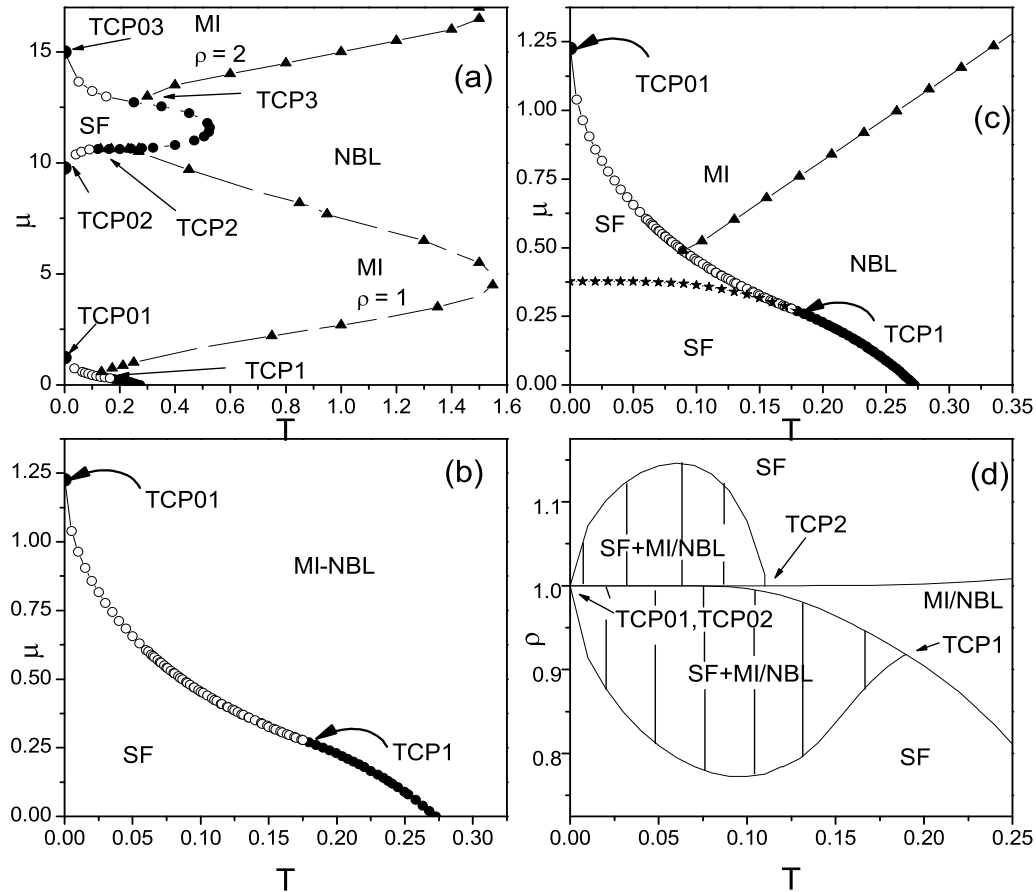
FIG. 4: (a) Mean-field phase diagram in the $\mu - T$ plane for $U_0 = 12$ and $U_2 = 0$. Lines with open (filled) circles represent first-order (continuous) SF-MI/NBL phase boundaries. First-order and continuous boundaries meet at tricritical points(TCP). The $T = 0$ ($T > 0$) tricritical points are labeled TCP01, TCP02, etc. (TCP1, TCP2, etc.). The line with triangles represents the crossover boundary between MI and NBL regions of the MI/NBL phase. The lower left corner of the phase diagram in (a) is enlarged in (b) and (c). The only difference between (b) and (c) is that the latter shows the MI-NBL crossover boundary (line with triangles) and a line with stars, the locus of points in the SF phase at which the variational free energy $\mathcal{F}$ goes from a curve with three minima to one with two minima; this line meets the SF-MI boundary at TCP1. (d) The density-temperature ($\rho - T$) version of part of the $\mu - T$ phase diagram of (a) (without the MI-NBL crossover line); tie lines are used to hatch the two-phase regions in which SF and MI/NBL phases coexist (see text).

from a curve with three minima to one with two minima. This line meets the SF-MI boundary at a tricritical point labeled TCP1. Higher islands of the SF phase show analogous tricritical points labeled TCP2, TCP3, etc.; the SF-MI phase boundaries meet the $T = 0$ axis at the zero-temperature tricritical points TCP01, TCP02, TCP03, etc. [Fig. 4 (a)]. Figure 4 (d) shows the density-temperature ($\rho - T$) version of part of the $\mu - T$ phase diagram of Fig. 4 (a) (without the MI-NBL crossover line); the first-order parts of the SF-MI boundaries now appear as regions of two-phase coexistence that are hatched with tie lines; the two-phase regions corresponding to the two

lowermost SF-MI boundaries in Fig. 4 (a) are depicted; they end at the tricritical points TCP1 and TCP2 out of which emerge the continuous (second-order) SF-MI phase boundaries. We use the label MI/NBL since there is no strict distinction between MI and NBL phases for $T > 0$. Note that, in such a $\rho - T$ phase diagram, the MI/NBL phases get pinched into exponentially small regions [e.g., in the vicinity of $\rho = 1$ in Fig. 4 (d)] as $T \to 0$ and two zero-temperature tricritical points get mapped onto each other [e.g., TCP01 and TCP02 in Fig. 4 (d)].

We now investigate the case $U_2 \neq 0$, so the onsite interaction between bosons depends on the spin. This

lifts some of the infinite degeneracy we encountered in the case $U_2 = 0$ as can be seen directly at $T = 0$ by comparing the pseudo-grayscale plots of $\mathcal{E}_0$ in Figs. 1 (b), (c), and (d), for $U_2 = 0$, $U_2 > 0$, and $U_2 < 0$, respectively.

If $U_2 < 0$ there are four degenerate minima of, each corresponding to a ferromagnetic SF, with $\psi_{-1} = \psi_1$ and $\psi_0 = \pm\sqrt{2}\psi_{\pm 1}$. The zero-temperature, mean-field, phase diagram for this case is shown in Fig. 5; it has the same topology as the phase diagram for the case $U_2 = 0$ [Fig. 1 (a)]. We see that the MI phases have shrunk marginally and the SF-MI transitions are still continuous. The continuous nature of the $T = 0$, SF-MI transition is illustrated by the continuous variation of $\psi_{\pm 1}, \psi_0$, and ρ_s as functions of μ in Fig. 6. The parameter $\langle \vec{F} \rangle^2$, defined only in the SF phase, assumes the value 1, which confirms that we have a ferromagnetic SF phase in this case. The $\mu - T$ phase diagram for the case $U_2 < 0$ has the same topology as the $U_2 = 0$ phase diagrams of Fig. 4. We do not show the $\mu - T$ phase diagram for $U_2 < 0$ since, for the parameters we use, namely, $U_0 = 12$ and $U_2/U_0 = -0.03$, the phase boundaries are very close to those in Fig. 4.

If $U_2 > 0$ there are four degenerate minima of the variational free energy $\mathcal{F}$ shown, e.g., at $T = 0$ in the pseudo-grayscale plot of Fig. 1. Each one of these minima corresponds to a polar SF, with either $\psi_{-1} = \psi_1 \neq 0$ and $\psi_0 = 0$ or vice versa as shown in the plots of $\psi_{\pm 1}$ and

ψ_0, versus μ in Fig. 7 for $U_2/U_0 = 0.03$. The parameter $\langle F \rangle$, defined only in the SF phase, assumes the value 0, which also confirms that we have a polar SF phase. The zero-temperature, mean-field, phase diagram for this case is shown in Fig. 8. If the density ρ is equal to an odd integer ($\rho = 1$ is shown in Fig. 8), this phase diagram has the same form as its counterpart for $U_2 = 0$ [Fig. 1 (a)]. We see that the MI lobes expand marginally, and the SF-MI transitions are still continuous. However, if the density ρ is equal to an even number ($\rho = 2$ is shown in Fig. 8), the SF-MI transition becomes first-order and the MI phase is stable over a much wider region of parameter space than for the case $U_2 = 0$: As we show in Fig. 9, for $U_2/U_0 = 0.03, U_0 = 7$ and $T = 0$, ρ_s and ρ vary continuously as functions of μ at the SF-MI transition for $\rho = 1$ but discontinuously for $\rho = 2$; for comparison we also include the analogous plots for $U_2 = 0$. [We use $U_0 = 7$ here, rather than $U_0 = 12$, to compress the range of μ over which the SF-MI transitions occur.]
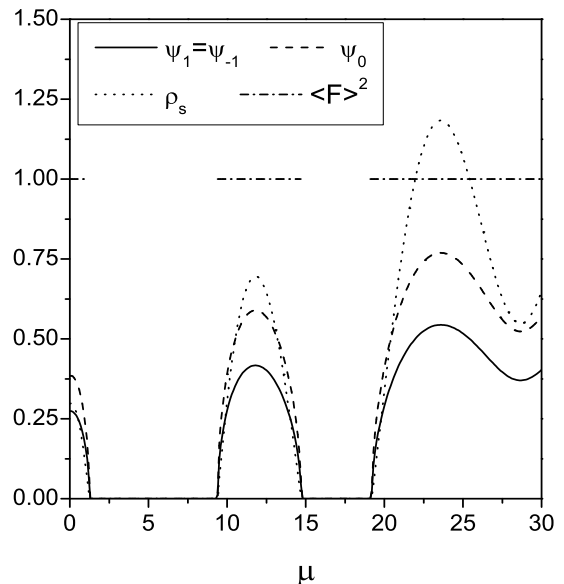
FIG. 6: Mean-field values of the superfluid order parameters $\psi_1 = \psi_{-1}$ and ψ_0 and ρ_s plotted as functions of μ for $U_0 = 12$, $U_2/U_0 = -0.03$, and $T = 0$; ρ_s goes to zero continuously at the SF-MI transitions. The parameter $\langle \vec{F} \rangle^2$, defined only in the SF phase, assumes the value 1, which confirms that we have a ferromagnetic SF phase in this case.

For $\rho = 2$ in the MI phase, there are exactly two bosons localized per site and the total spin at every site can be either $S = 0$ or $S = 2$. Since $U_2 > 0$ there is an energy difference between the $S = 0$ and $S = 2$ states, with a lower energy for the singlet state. To go from the MI to the SF phase, this singlet state has to be broken by supplying an energy $\sim U_2$, which gives a rough estimate for the *latent heat* of this first-order transition if $0 \lesssim T$. This
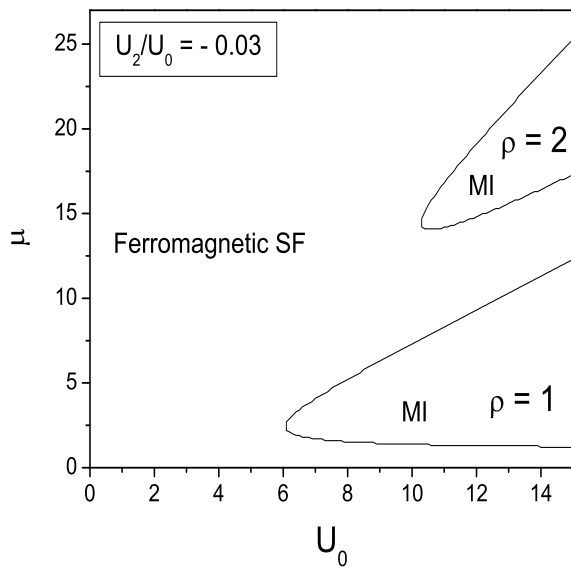

FIG. 5: Mean-field phase diagram in the $(\mu - U_0)$ plane for $U_2/U_0 = -0.03$ and $T = 0$. This has the same topology as the phase diagram for the case $U_2 = 0$ [Fig. 1 (a) for $T = 0$] but the MI lobes have shrunk marginally; the SF-MI transitions are continuous.

requirement of a latent heat leads to the greater stability of the MI phases for even values of ρ relative to their counterparts for odd values of ρ. Thus the $\rho = 2$ MI lobe in Fig. 8 is substantially larger than the one for $\rho = 1$. The $\mu - T$ phase diagram for the case $U_2 > 0$, shown in Fig. 10 (a), for $U_0 = 12$ and $U_2/U_0 = 0.03$, has nearly the same form as the $U_2 = 0$ phase diagram of Fig. 4. The principal qualitative difference between these phase diagrams is that, if $U_2 > 0$, there are no zero-temperature, tricritical points for the first-order boundaries associated with the MI lobes for even values of ρ; e.g., the tricritical point TCP03 in Fig. 4 has no counterpart in Fig. 10 (a). A quantitative comparison between these two phase diagrams is made in Fig. 10 (b); this shows that the two phase diagrams are nearly indistinguishable except for the first-order boundaries that link the zero-temperature, SF-MI transitions for even values of ρ with the tricritical points directly above them (e.g., TCP3). In Fig. 10 (b) the dashed line with open circles (open diamonds) is the first-order boundary for $U_2/U_0 = 0.03$ ($U_2 = 0$); the region **I** between these lines lies in the MI (SF) phase if $U_2/U_0 = 0.03$ ($U_2 = 0$); the lines with filled triangles show the MI-NBL crossover as in Fig. 4 (a). Phase diagrams such as Fig. 10 are obtained by calculating the order parameters ψ_σ, and thence ρ and ρ_s, as functions of μ at different temperatures. Representative plots are shown in Fig. 11 for $U_2/U_0 = 0.3, U_0 = 7$, and $T = 0$ and $T = 0.05$.

FIG. 8: Mean-field phase diagram in the $(\mu - U_0)$ plane for $U_2/U_0 = 0.03$ and $T = 0$. The $\rho = 1$ MI lobe has the same form as its counterpart for $U_2 = 0$ [Fig. 1 (a)]. We see that the MI lobes expand marginally, and the SF-MI transitions are continuous (represented by a continuous line); but for $\rho = 2$ the SF-MI transition becomes first-order (represented by a dashed line) and the MI phase is stable over a much wider region of parameter space than for the case $U_2 = 0$.

IV. CONCLUSIONS

We have carried out the most extensive study of the phase diagram of the spin-1 Bose Hubbard model so far by generalizing an intuitively appealing mean-field theory that has been used earlier for the spinless case. Our study yields both zero-temperature and finite-temperature phase diagrams for this model. Only $T = 0$ phase diagrams had been obtained so far[9,10,11]; so our elucidation of the finite-temperature properties of this model yields qualitatively new insights. We find, in particular, that several of the SF-MI transitions in this model are generically first order; at sufficiently high temperatures they become continuous via tricritical points. Tricritical points also abound at zero temperature since some, but not all, of the finite-temperature, first-order transitions become continuous as $T \rightarrow 0$. The resulting phase diagrams (Figs. 4 and 10) are very rich and should provide a challenge for experimental studies, which we hope our work will stimulate. Experiments can study both the case $U_2 < 0$, which can be realized possibly by using ^{87}Rb, and the case $U_2 > 0$, which can be realized by using ^{23}Na. Thus, in principle, both the phase diagrams of Figs. 4 and 10 could be obtained experimentally. Of course this will require good experimental control of both
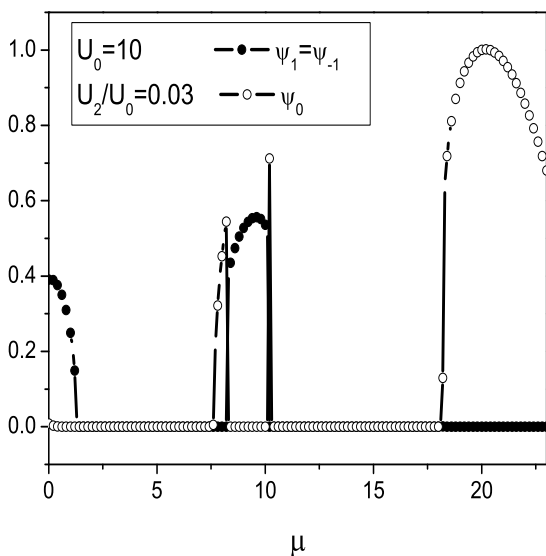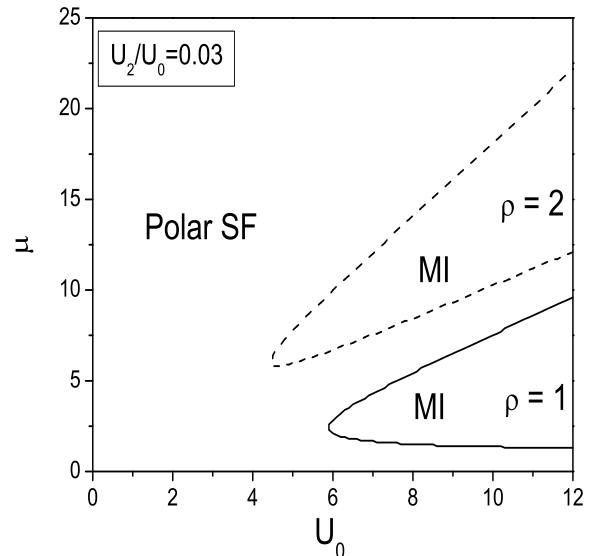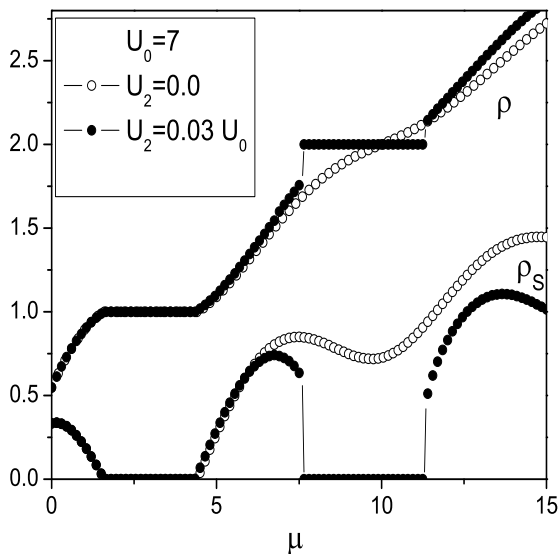

FIG. 7: Mean-field values of the superfluid order parameters $\psi_1 = \psi_{-1}$ and ψ_0 plotted as functions of μ for $U_0 = 10$, $U_2/U_0 = 0.03$, and $T = 0$. The SF phase has either $\psi_{-1} = \psi_1 \neq 0$ and $\psi_0 = 0$ or vice versa, which confirms that we have a polar SF in this case.

the temperature and the density (or chemical potential) of the bosons.

Our mean-field theory has been designed to investigate the relative stabilities of SF and MI/NBL phases. It has enough structure to unravel the differences between polar and ferromagnetic supefluids. However, our mean-field theory does not account for order parameters that can distinguish between different spin orderings in the MI phase, e.g., spin-singlet and nematic MIs, which have been investigated in the limit $U_0 \to \infty$ by some groups[14,15]. The generalization of our mean-field theory to include such types of structures in the MI phases of model (1) lies beyond the scope of this study but is an interesting challenge for further theoretical work.

FIG. 9: Plots of ρ_s and ρ as functions of μ for $T = 0$, $U_0 = 7$, and $U_2/U_0 = 0.03$ (filled circles) and $U_2 = 0$ (open circles). In the former case ρ_s changes continuously at the SF-MI transitions at the boundary of the $\rho = 1$ MI lobe (Fig. 8) but jumps at the first-order SF-MI transitions associated with the boundary of the $\rho = 2$ MI lobe. For $U_2 = 0$ only the $\rho = 1$ lobe is encountered in this plot and the SF-MI transitions are continuous; ρ_s shows a gentle minimum in the vicinity of the $\rho = 2$ MI lobe.

* Electronic address: rvpai@unigoa.ac.in
† Electronic address: kshesh@gmail.com
‡ Electronic address: rahul@physics.iisc.ernet.in; URL: http://www.physics.iisc.ernet.in/~rahul; also at Jawaharlal Nehru Centre for Advanced Scientific Research, Jakkur, Bangalore 560 064, India.
1 F. Dalfovo, S. Giorgini, L. P. Pitaevskii and S. Stringari, Rev. Mod. Phys. **71** 463 (1999); I. Bloch, J. Dalibard, and W. Zwerger, arXiv:0704.3011bv1 [cond-mat.other]; M. Lewenstein, *et al*, arXiv:cond-mat/0606771.
2 Subir Sachdev, Quantum Phase Transitions, (Cambridge University Press, Cambridge, 1999).
3 M. Greiner, O. Mandel, T. Esslinger, T. W. Hänsch and L. Bloch Nature (London) **415** 39 (2002).
4 D. Jaksch, C. Bruden, J. I. Cirac, C. W. Gardiner and P. Zoller Phys. Rev. Lett. **81** 3108 (1998).
5 K. Sheshadri, H. R. Krishnamurthy, R. Pandit, and T. V. Ramakrishnan Europhys. Lett. **22** 257 (1993); Phys. Rev. Lett. **75** 4075 (1995).
6 D. M. Stamper-Kurn *et al* Phys. Rev. Lett. **80** 2027 (1998).
7 T. L. Ho, Phys. Rev. Lett. **81** 742 (1998).
8 S. Mukerjee, C. Zu, J.E. Moore, Phys. Rev. Lett. **97** 120406 (2006).
9 S. Tsuchiya, S. Kurihara and T. Kimura Phys. Rev. Lett., **94** 110403 (2005).
10 K. V. Krutitsky and R. Graham, Phys. Rev. A, **70** 063610 (2004).
11 R.V. Pai, K. Sheshadri, and R. Pandit , in Current Topics in Atomic, Molecular, and Optical Physics, eds. C. Sinha and S. Bhattacharyya (World Scientific, Singapore, 2007) pp. 105 - 119.
12 C. K. Law, H. Pu and N. P. Bigelow Phys. Rev. Lett. **81** 5257 (1998).
13 We have checked that this value of n_{max} suffices for the large values of U_0 we use by comparing our results with those for $n_{max} = 2$ and 3.
14 A. Imambekov, M. Lukin and E. Demler, Phys. Rev. A **63** 063602 (2003).
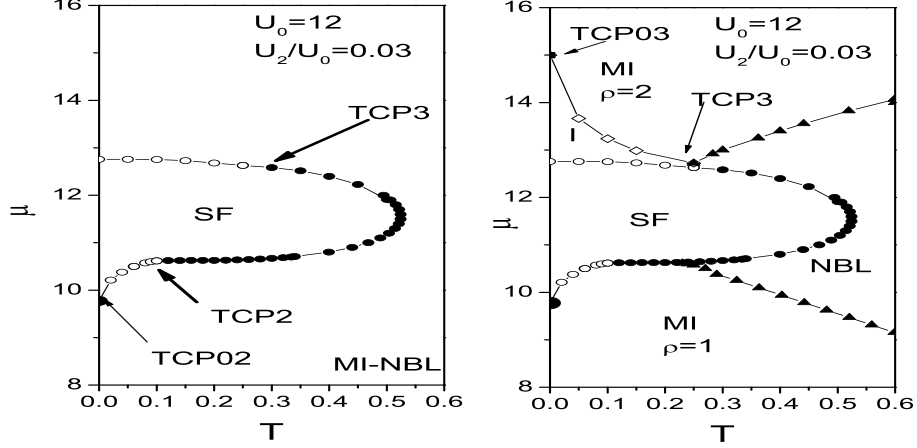15 G. Fáth and J. Sólyom, Phys. Rev. B **51** 3620 (1995).

FIG. 10: (a) Mean-field phase diagram in the $(\mu - T)$ plane for $U_0 = 12$, $U_2/U_0 = 0.03$ showing first-order (open circles) and continuous (filled circles) transitions between SF and MI/NBL phases and tricritical points (TCP). This phase diagram is nearly the same as the $U_2 = 0$ phase diagram [Fig. 4], but there are no zero-temperature, tricritical points for the first-order boundaries associated with the MI lobes for even values of ρ: e.g., TCP03 in Fig. 4 has no counterpart here. (b) A quantitative comparison between these two phase diagrams shows that the two phase diagrams are nearly indistinguishable except for the first-order boundaries that link the zero-temperature, SF-MI transitions for even values of ρ with the tricritical points directly above them (TCP3 here); lines with open circles (open diamonds) denote the first-order boundaries for $U_2/U_0 = 0.03$ ($U_2 = 0$); the region **I** between these lines lies in the MI (SF) phase if $U_2/U_0 = 0.03$ ($U_2 = 0$); the lines with filled triangles show the MI-NBL crossover boundary.
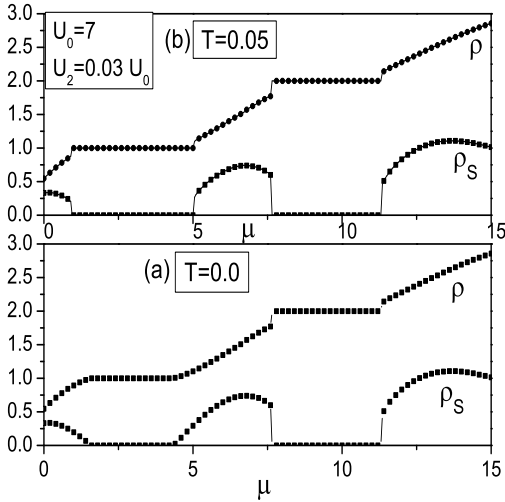

FIG. 11: Representative plots of ρ_s and ρ versus μ for (a) $T = 0$ and (b) $T = 0.05$ for $U_0 = 7$, $U_2/U_0 = 0.03$ showing jumps at first-order SF-MI transitions; ρ_s changes continuously at the $T = 0$, continuous SF-MI transition associated with the $\rho = 1$ MI lobe.